iScience

CellPress
OPEN ACCESS

Article

In vivo laser speckle contrast imaging of microvascular blood perfusion using a chip-on-tip camera

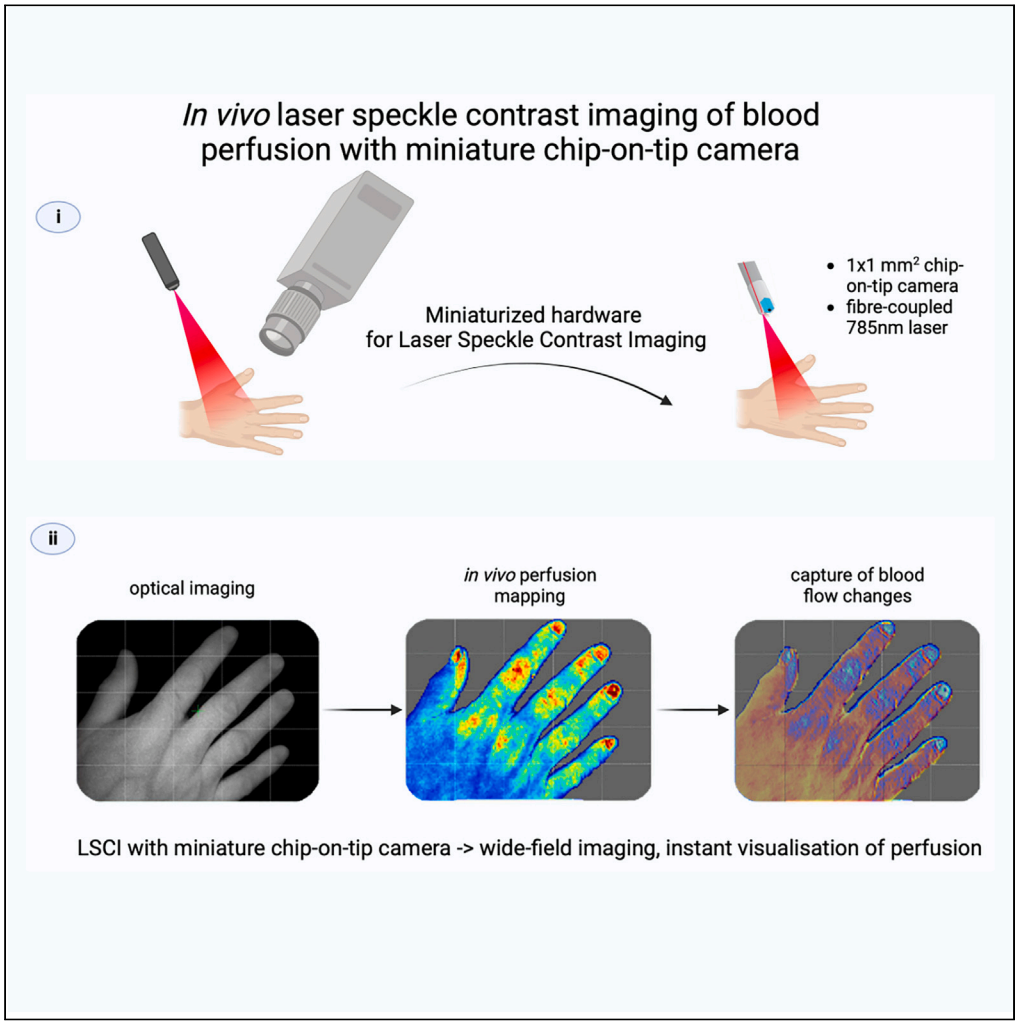

Lukas Markwalder, Rodney Gush, Faisel Khan, Colin E. Murdoch, Nikola Krstajić

c.z.murdoch@dundee.ac.uk (C.E.M.)
n.krstajic@dundee.ac.uk (N.K.)

Highlights

Laser speckle contrast imaging with miniature 1mm^2 chip-on-tip camera

Chip-on-tip camera achieved detailed blood perfusion maps

Instant measure of perfusion changes by miniature LSCI system confirmed *in vivo*

Potential to translate wide-field LSCI technology to aid key-hole surgery

Markwalder et al., iScience 27, 109077
March 15, 2024 © 2024
https://doi.org/10.1016/j.isci.2024.109077

iScience

CellPress
OPEN ACCESS

Article

In vivo laser speckle contrast imaging of microvascular blood perfusion using a chip-on-tip camera

Lukas Markwalder,[1] Rodney Gush,[2] Faisel Khan,[1] Colin E. Murdoch,[1,4,5,*] and Nikola Krstajić[3,4,*]

SUMMARY

Laser speckle contrast imaging (LSCI) is an important non-invasive capability for real-time imaging for tissue-perfusion assessment. Yet, the size and weight of current clinical standard LSCI instrumentation restricts usage to mainly peripheral skin perfusion. Miniaturization of LSCI could enable hand-held instrumentation to image internal organ/tissue to produce accurate speckle-perfusion maps. We characterized a 1mm^2 chip-on-tip camera for LSCI of blood perfusion *in vivo* and with a flow model. A dedicated optical setup was built to compare chip-on-tip camera to a high specification reference camera (GS3) for LSCI. We compared LSCI performance using a calibration standard and a flow phantom. Subsequently the camera assessed placenta perfusion in a small animal model. Lastly, a human study was conducted on the perfusion in fingertips of 13-volunteers. We demonstrate that the chip-on-tip camera can perform wide-field, *in vivo*, LSCI of tissue perfusion with the ability to measure physiological blood flow changes comparable with a standard reference camera.

INTRODUCTION

Laser speckle contrast imaging (LSCI) is a clinical technique for non-invasive assessment of blood flow activity in the superficial layers of tissue[1] that is still not widely used compared with other imaging techniques such as MRI or ultrasound. LSCI strength lies in wide-field (i.e., imaging of an area of tissue into a camera frame), imaging of spatial and temporal perfusion without the requirement for invasive contrast agents. LSCI allows clinicians to locate areas of poor perfusion or to observe hyperperfusion in quasi real time due to the relatively low computational burden of converting image data into perfusion maps.[2]

Furthermore, the technology relies on a relatively simple and low-cost laser and camera setup. Since its introduction in the early 1980s for imaging retinal vasculature,[3] LSCI has been used for various blood flow assessments, predominantly in easy-to-access areas of skin or surgically exposed tissue due to size of the current LSCI imaging systems (e.g., moorFLPI-2, Moor Instruments Ltd, UK). Laser speckle imaging has been effectively implemented in breast reconstructive surgery.[4]

Perfusion imaging can be performed using many techniques, from magnetic resonance imaging (MRI) and computed tomography (CT), via ultrasound and optical methods.[5,6] We confine our attention to clinically proven optical techniques because they provide instantaneous and affordable health of tissue intraoperatively. For example, it is usually not practical to operate during MRI or CT scanning. Contrast enhanced ultrasound (CEUS) is a recent candidate for perfusion imaging with depth, but it is more limited in terms of imaging resolution and size of vessels (~2mm).[7] Laser Doppler, another laser-based perfusion imaging method, has been approved by UK National Institute for Health and Care Excellence (NICE) for effective burn wound assessment[8] as part of the clinical pathways to alert cases that need further surgical treatment. The method relies on pixel-after-pixel scanning, slower than LSCI wide-field imaging.

As mentioned previously, we focus on LSCI and several studies have addressed the integration of the LSCI technique into an endoscope and demonstrated perfusion imaging, e.g., in the knee,[9] uterus,[10] gastrointestinal tract,[11,12] and deep brain.[13] While these studies highlighted the potential of LSCI for intra-surgery imaging, they relied on combining research grade (or standard vision) cameras with rigid endoscopes[9–12] or, in limited way, fiber image guides.[14] Direct-view into brain using miniature optics was used for deep brain imaging, but with highly disruptive endoscopy.[13] The best performance achieved so far is from rigid endoscope architectures since there is a clear optical path from tissue to camera. However, while rigid endoscopes provide a form of miniaturization, they cannot be used in all clinical pathways (e.g., pulmonology, urology, cardiology, and gastroenterology) which regularly view internal organs/tissue using flexible endoscopes inserted through natural channel (e.g., airway, gastrointestinal tract). Fiber guides (or fiber bundles) are a natural candidate as a flexible guide into

[1]Systems Medicine, School of Medicine, University of Dundee, Ninewells Hospital & Medical School, DD1 9SY Dundee, UK
[2]Moor Instruments, Millwey Rise Industrial Estate, Weycroft Avenue, EX13 5HU Axminster, UK
[3]School of Science and Engineering, Fulton Building, University of Dundee, DD1 4HN Dundee, UK
[4]These authors contributed equally
[5]Lead contact
*Correspondence: c.z.murdoch@dundee.ac.uk (C.E.M.), n.krstajic@dundee.ac.uk (N.K.)
https://doi.org/10.1016/j.isci.2024.109077

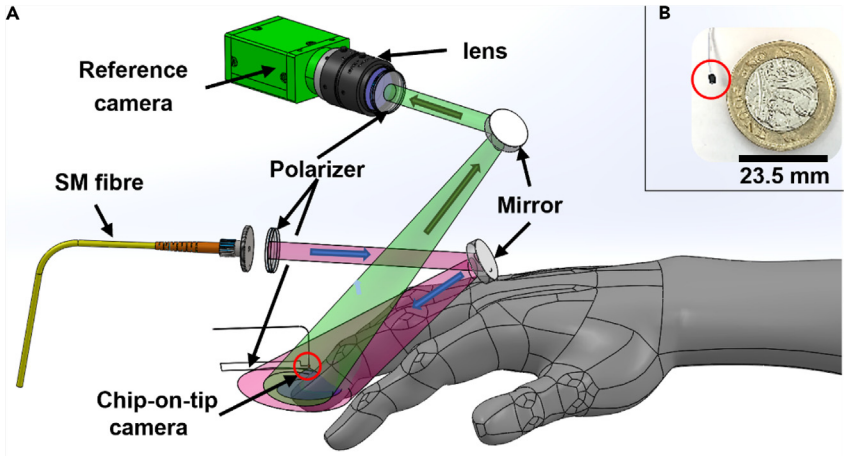

Figure 1. Optical layout of the LSCI imaging system

(A) Schematic diagram of LSCI imaging setup. Illumination by a 785 nm, fiber-coupled laser and imaging with the chip-on-tip camera (NanEye, AMS) and a reference camera (FLIR). Chip-on-tip camera was 13 mm from object.

(B) Size comparison of Chip-on-tip camera (1 mm × 1 mm size) to a one-pound coin.

tissue of interest. However, they have the disadvantage of splitting the view into a mosaic of numerous fiber cores with gaps from fiber cladding.[15] Furthermore, the properties of fiber cores limit how speckles are transmitted and detected[16] since the number of modes transmitted will vary from core to core.

In the present study, we implement a commercially available miniature (1 mm × 1 mm) chip-on-tip camera with integrated lens (NanEye, grayscale version, AMS, Austria) into an LSCI setup and demonstrate feasibility of LSCI imaging performance in compact format. The main reasons we chose this camera are as follows: (i) camera is readily available and affordable from several suppliers; (ii) the CMOS (complimentary metal-oxide semiconductor) sensor has a track record in endoscopy applications due to optimized wafer-level microlensing (see in the following discussion section); (iii) grayscale version of the CMOS sensor is available for optimal speckle imaging whereas white light endoscopy normally uses color balanced CMOS sensor with Bayer filter.

Prior use of this or similar cameras include point-based laser speckle sensing for gingival health,[17] preliminary speckle imaging of skin,[18] wearable fibreless mouse brain blood flow imager.[19] Whereas these applications were able to track physiological perfusion changes from a single point, our design preserves the wide-field (or area) imaging aspect of LSCI. Commercial available LSCI and LDI systems are routinely used in pre-clinical small-animal models for assessment of peripheral artery disease, stroke, and vascular function.[20–22] The ability to image perfusion in different organs in small animals has led to advances in miniature microscopes,[23–26] which provide a miniaturized platform for wide-field LSCI,[27] scanning laser Doppler vibrometer, and multi-modal imaging.[28] While many cameras and lasers were evaluated for LSCI,[29–31] it is indeed surprising to find that chip-on tip camera has not been more widely evaluated for flexible endoscopy with wide-field-view and LSCI especially since the chip-on-tip CMOS cameras have been available for more than a decade. Our main aim in this paper is to prove the technology is suitable for full implementation into flexible endoscopy as a wide-field or area imaging device that can enhance endoscopic surgery. Our setup is not fully miniaturized and endoscopic (see Figure 1 where optical fiber and camera are separately placed while they should be integrated into single housing for endoscopy), but given the results presented—we demonstrate the current chip-on-tip camera technology with integrated optics, which is capable to be integrated into flexible endoscopes, has the ability to image changes in perfusion over a small but wide-field area. We present diagrams for the endoscopy system in discussion and Figure S2 below.

The speckle patterns captured by our setup allow for computation of perfusion maps over an area 4.9 mm^2, at a 13mm working distance (see Table 1 for chip-on-tip details). *In vivo* measurements on the human fingertip and vascular mapping of murine fetus yielded detailed perfusion images. Small-animal *in vivo* models of pregnancy complications are an important aspect of understanding the physiological processes involved. For example, mapping vasculature and perfusion of placenta allows for a powerful test during twin-to-twin transfusion syndrome procedure.[10] Capture and analysis of speckle patterns is also an established imaging method in ultrasound context[32] and we re-deploy it optically. Hence, this setup exploits the imaging function of (commercial) LSCI imagers while reducing the size of the required hardware components to enable assessment of internal organs or tissues or orifices within the body. With future integration of fibre-coupled laser source and the chip-on-tip camera into a custom housing we would pave the way to a flexible endoscope architecture.

RESULTS

Calibration of laser speckle contrast imaging

An optical-LSCI setup (Figure 1A) was constructed to allow quasi-simultaneous acquisition from the chip-on-tip (Figure 1B) and reference (GS3-U3-32S4M-C 1/1.8″ FLIR Grasshopper3 High Performance USB 3.0 Monochrome Camera, Teledyne FLIR, USA) camera (Table 2). Measurements of the optical-LSCI setup on a reference target allowed for calibration and the conversion of speckle contrast to standardized

Table 1. Technical specifications of the cameras

Camera	Reference camera (GS3)	Chip-on-tip camera (NanEye)
Product code	GS3-U3-32S4M-C	NE2D_B&W_FOV90F2.7_2m
Manufacture	Teledyne FLIR, US	AMS, Austria
Function	Monochromatic (CMOS) standard machine vision camera used for reference	Monochromatic (CMOS) micro camera with 1 × 1 × 1.69 mm module size
Optical format	1/18″	1/16″
Pixel size	3.45 μm × 3.45 μm	3 μm × 3 μm
CMOS sensor resolution (number of pixels in detector array)	2048 × 1536 pixel	249 × 250 pixel
Lens system	50 mm fixed focal length (MVL50M23, Thorlabs)	f/# is 2.7, focal length for assumed 1 mm aperture is 2.7 mm
Camera target distance	350 mm	13 mm
Temporal dark noise	5.11 e^-	50.75 e^-
Exposure (@40 frames per second)	25 ms	25 ms

fps, frames per second.

perfusion units (PU). A static reference, equivalent to zero perfusion activity, yielded spatial contrast of 0.442 ± 0.010 for the reference camera and 0.233 ± 0.007 for chip-on-tip under 5mW illumination. For the motility target which is based on Brownian motion and equivalent to 500 PU, a spatial contrast value of 0.165 ± 0.005, and 0.075 ± 0.006 were measured for reference and chip-on-tip cameras, respectively. Both cameras show a clear distinction in spatial contrast values between the static and motility reference which was later used for calibration of *in vivo* measurements. However, contrast captured by the chip-on-tip camera is notably lower because of reduced sensor sensitivity and a lower pixel number compared to the reference camera (Table 1).

Chip-on-tip laser speckle contrast imager can detect linear flow

Temporal LSCI measurements of linear flow were obtained using a custom-built flow phantom with circular 0.75 mm diameter channels embedded in an intralipids-agarose bed (Figure 2A). A temporal contrast line profile was computed, across the gel bed and orthogonally cutting one of the channels (Figure 2B). The monochromatic images of chip-on-tip and the reference camera show the relative position of the line profile. There was a clear blurring of the speckle pattern over and around the channel, compared with the more developed pattern of the static area (gel bed). Temporal contrast, captured by the reference camera, was 1.5 ± 0.1 for the static area and gradually decreased toward the center of the channel, with a minimum of 0.95 (Figure 2B). The chip-on-tip tracked the profile of the reference camera, although with a general reduction in contrast (Figure 2B). Imaging the static gel area yielded values between 0.48 and 0.53 and a minimum of 0.41 for the center of the channel area. The line profiles show reduced contrast for blurred speckle pattern of areas with channel flow. Conversely, speckle contrast is higher for the background. Values larger than one, recorded by the reference camera, are an artifact of adjusting the computed contrast values by multiplication with the intensity read of the pixels involved in the contrast kernels and normalization by the average frame intensity.

Temporal contrast of the flow of an intralipid solution through the channels (0.75 mm) was obtained for multiple flow speeds (0.1, 0.1, 5, 10 m/s) (Figure 2C). Contrast values were area-averaged in a box of 200 × 50 pixels for the reference camera and 100 × 30 pixels for chip-on-tip. Both cameras showed a similar exponential decay (exponent −0.048, −0.044 for the reference camera and chip-on-tip, respectively) in temporal contrast with increasing flow speed. For the reference camera, temporal contrast was 0.158 ± 0.013 for 0.1 mm/s and decreased to 0.127 ± 0.013 for 10 mm/s flow. For chip-on-tip, the values were off-set and generally 0.1 lower with temporal contrast of 0.064 ± 0.008 for 0.1 mm/s and 0.052 ± 0.008 for 10 mm/s. Temporal contrast of both cameras correlated linearly. The linear regression model yielded $R^2 = 0.956$ (Figure 2D).

Perfusion mapping in a murine model

In the context of cardiovascular research of pregnancy complications, vascular/perfusion mapping with the developed LSCI setup was tested *in vivo* on a murine pre-clinical model of pregnancy. Figure 3 shows perfusion maps of two surgically exposed murine fetus *in utero* (located within the amnionic membrane) during late gestation (day 17.5) with the individual placentas and the maternal supply by the uterine artery. The temporal LSCI scans display the perfusion maps under normal condition (Figure 3B) and under ligation of blood vessels supplying the pups (arrows in Figure 5C indicate the point of restriction). A clear decrease in perfusion activity by 23 ± 2% was observed by both cameras when blood flow was restricted (Figure 3C). Despite imaging through the amnionic membrane, the scans also revealed placental perfusion, marked by the black box. The scans also showed varying blood flow in the vessels, as seen in the top quarter of the perfusion images. Thus, the

Table 2. Protocol of altering blood flow in the arms of volunteers with LSCI measurements on the fingertip

Step	Action
Baseline 1-4	4 measurements each with chip-on-tip and Reference cameras
Occlusion 60 mmHg	upper arm occlusion, hold for 30 s and scan
Occlusion 120 mmHg	upper arm occlusion, hold for 30 s and scan
Occlusion 180 mmHg	upper arm occlusion, hold for 30 s and scan
	Recovery for 10 min
Recovery scan 1	
Occlusion 180 mmHg	upper arm occlusion, hold for 60 s and scan
	Recovery for 10 min
Recovery scan 2	
Water bath	Hand in warm water bath (>40°C) for 5min
Temperature 1-3	Scans after 30 s, 1 min and 2 min after exiting water bath

Scans were conducted subsequently within a 5-s window, with chip-on tip followed by Reference camera.

measurements highlight the chip-on-tip system's capability of vascular mapping by providing detailed images of tissue perfusion and indication of flow within macroscopic vessels in a pre-clinical or surgical setting. The scans also indicated the potential of a future chip-on-tip camera endoscope integration for intra-surgery LSCI, to measure visceral tissue blood flow *in situ*.

Blood perfusion study in human fingertip yields promising results for future chip-on-tip LSCI

To test if the LSCI hardware was sensitive enough to measure physiological blood flow changes in the dermal vasculature we measured perfusion at the fingertip in volunteers (male and female aged 20–60 years) under varying conditions. Sequential LSCI scans on the fingertip by the reference and chip-on-tip cameras during increasing upper-arm occlusion demonstrated clear stepwise decrease in relative finger-tip perfusion correlating with the increasing cuff pressure (60, 120, and 180 mmHg) (Figure 4A). The red square in the images (Figure 4A) defines the region of interest used for the calculations of relative perfusion, as normalized to baseline measurements, under various conditions (Figure 4B). Occlusion of 60, 120, and 180 mmHg induced an average 16 $\pm$ 2%, 31 $\pm$ 4%, and 39 $\pm$ 3% reduction, respectively, in relative finger-tip perfusion captured by the reference camera. In comparison, the chip-on-tip captured similar values compared to the reference camera with perfusion reductions of 15 $\pm$ 3%, 38 $\pm$ 4%, and 54 $\pm$ 4% for the same cuff pressures. The cuff was then deflated and after a 10 min recovery period, perfusion was back to baseline level as observed by both cameras. A rapid occlusion at 180 mmHg achieved a similar reduction in blood flow activity as seen previously with the stepwise cuff inflation. Likewise, the subsequent 10 min of recovery was also similar. To measure vasodilation and subsequent mild changes in perfusion activity, the subject's hands were warmed in a water bath with temperature >40 $\pm$ 2°C for 5 min. A scan within 30 s after removing from the bath yielded perfusion values 5.5 $\pm$ 1.5% higher than baseline for the reference camera, and 17 $\pm$ 4% for chip-on-tip. Additional measurements after 1 and 2 min observed perfusion level decrease to 4 $\pm$ 2% above baseline, respectively, and 11 $\pm$ 4% for the chip-on-tip. Generally, the relative (PU converted and baseline-normalized) spatial contrast values captured by chip-on-tip and the reference camera correlated well through the applied protocol ($R^2 = 0.98$). Interestingly, the chip-on-tip camera observed higher amplitudes of perfusion flow changes, i.e., relative perfusion levels was lower for full occlusion than for the reference camera. Similarly, temperature stimulation resulted in higher values for chip-on-tip than for the reference image data. However, to note is the general reduction in measured contrast. Like the measurements on the calibration kit, the recorded values for chip-on-tip were approximately half the magnitude of the reference camera which may be explained by lower resolution and sensitivity of the chip-on-tip CMOS sensor.

Figure 5 shows Bland-Altman plot which provides further analysis of the correlation between the reference camera and chip-on-tip camera. Both cameras had good correlation during most of the protocol with values lying within the limits of agreement (average difference $\pm 1.96 \times$ standard deviation of difference). The Bland-Altman plot also highlights that chip-on-tip camera captured lower relative blood flow during occlusion than the reference camera and registered higher values during temperature stimulation (as observed in Figure 4B).

Limitations

The limitations in imaging optics were related to the small size and design of the chip-on-tip camera. The camera module incorporated a fixed lens with 90° FOV and f/# (or f-number) 2.7. At best focus (specified by the manufacturer), the camera was positioned at 13 mm distance to the imaging plane, a distance ideal for perfusion mapping. The fixed design, however, limited the degrees of adjustment for speckle imaging, particularly for matching speckle size with pixel size. The size of the smallest resolvable speckles is defined by

$$S_{min} = 2.44 \times (1 + M) \times f/\# \times \lambda, \quad \text{(Equation 1)}$$

Where M is the magnification of the imaging system, $f/\#$ is the f-number and λ the operating wave length.[33] N describes the ratio of the minimally resolvable speckle size and the pixel size of the imaging CMOS sensor. We computed $N_{chip\text{-}on\text{-}tip} = 1.54$ and $N_{G3} = 13.04$. For fulfillment

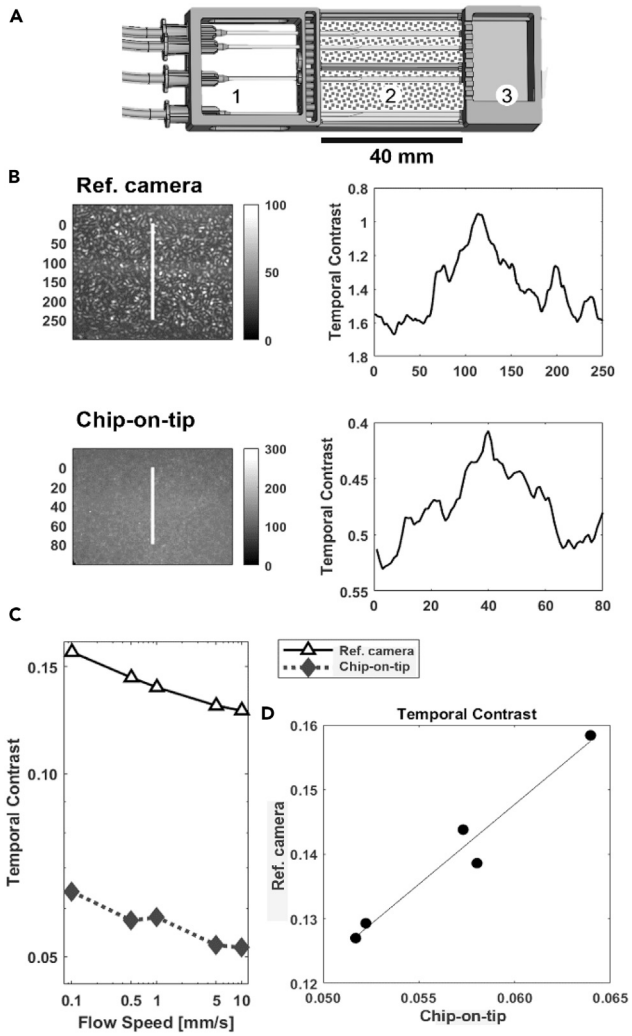

Figure 2. Temporal speckle contrast of linear flow in a flow phantom

Temporal speckle contrast of linear flow in a flow phantom (1% intralipid emulsion flowing through 0.75 mm diameter channels in a bed of 5.5% agarose [w/v] and 0.5% intralipid [v/v]).

(A) Schematic of the flow phantom with inlet (1), agarose bed with embedded channels (2) and a fluid collection reservoir (3).

(B) Line profile of computed temporal contrast (25 frames kernel, pixel-intensity-normalized) across a channel embedded in the gel bed. Comparison between captures of the chip-on-tip and the standard vision reference camera.

(C) Flow speed dependence of temporal speckle contrast measured by both cameras.

(D) Correlation of the speckle values (in B) captured by both cameras: a linear correlation model yields $R^2 = 0.958$.

of the Nyquist sampling criterion, $N \geq 2$ is required. Clearly, our chip-on-tip based system did not meet this standard and which impaired the quality of contrast imaging. As for under-sampling ($N < 2$), the captured speckle pattern of larger speckles interferes with smaller, non-resolvable speckles. Therefore, the absolute contrast is reduced as shown previously in a study by Ramirez-San-Juan et al.[34] However, the same study also showed that flow changes still could be captured consistently with $N < 2$. Thus, our speckle contrast imaging system based on a 1 mm^2 chip-on-tip camera demonstrated the perfusion imaging capability.

DISCUSSION

Speckle contrast comparison between chip-on-tip and reference cameras

For all data obtained, there were generally lower values of speckle contrast obtained by chip-on-tip than by the reference camera. The chip-on-tip camera's absolute contrast was on average just 59% of the level obtained by the reference camera during calibration, 49% for the flow phantom measurements, 50% for the finger blood flow study and 12% for murine uterine scans. Though lower in absolute values, the chip-on-tip camera tracked the standard vision camera reference well for changes in perfusion. Linear regression models showed $R^2 = 0.956$

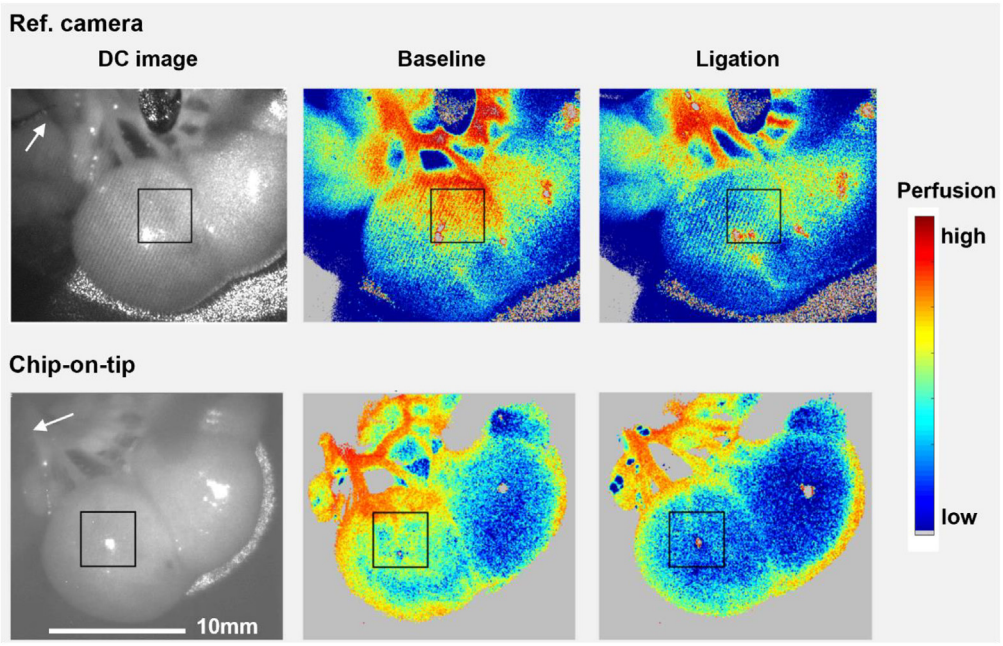

Figure 3. *In vivo* laser speckle imaging of placental perfusion using a chip on tip camera

Comparison of vascular/perfusion mapping in the reference camera (top) and chip-on-tip camera (bottom) of mice fetus with the custom LSCI setup under basal and ligated conditions. Imaging of perfusion of two pups, each in the amnionic membrane with its placenta (area of the black box). Imaging of baseline condition and during ligation of one of the supplying arteries (arrow in DC image). Ligation shows a general reduction of perfusion. Also visible with LSCI is blood flow in the larger blood vessels (top of scan images).

correlation for measurements on the flow phantom and 98% for the altered perfusion in the finger. We identified two main factors leading to the lower absolute contrast levels of chip-on-tip: sensor quality and limitations in imaging optics. As for noise, it affected the chip-on-tip camera more than the standard vision camera reference. Experimentally measured 50.75 e^- of temporal dark noise contributed 7.6× more to the signal (relative to grayscale value or digital number [DN]) than the 5.11 e^- of the reference camera (where e^- represent a photon generated electron as per European Machine Vision Association standard 4.0). In addition to the higher noise levels, the light-to-signal conversion was less efficient with a 24% quantum efficiency compared to 35% (both values derived from quantum efficiency vs. wavelength curves provided by manufacturers and therefore wavelength adjusted for 785 nm). As for limitations in imaging optics, the chip-on-tip camera relied on an integrated lens which locked the imaging specification. The reference camera, however, could be paired with a lens suitable for speckle imaging. Therefore, the ration of the minimally resolvable speckle size and the pixel size was much lower for the chip-on-tip with 1.54 compared to the 13.04 of the reference camera, leading to imaging of less developed speckle patterns.

Our objective was to validate the extent of camera miniaturization that is possible (and commercially available) while still being able to conduct robust LSCI. In doing so we evaluated a chip-on-tip CMOS camera and fiber-coupled laser illumination for *in vivo* perfusion imaging demonstrating its future ability to be developed into an integrated endoscopic LSCI system. We developed a test rig for the 1mm^2 chip-on-tip camera, a 785 nm SM-laser and the standard vision reference camera (G3) and conducted a series of flow phantom and *in vivo* tests. Measurements on a calibration target yielded reference values of spatial contrast for static condition and omnidirectional Brownian motion. The obtained range allowed for conversion of spatial speckle contrast into standardized PU, a measure which was used to quantify perfusion changes during a study of induced changes measured on the fingertip: during restriction by inflating a pressure cuff placed around the upper arm, and after warming the hand in a heated water bath. Through the application of a protocol and simultaneous imaging with the reference and chip-on-tip camera, we demonstrated that the chip-on-tip camera was able to accurately capture changes in perfusion. The chip-on-tip based system demonstrated that it could detect pronounced changes, i.e., baseline condition vs. maximum blood flow restriction, moreover the chip-on-tip camera was sensitive enough to measure perfusion changes as occlusion pressure increased, and the rapid changes in perfusion in response to change in temperature over 1–2 min time period. No significant difference was found for measurements by the 1mm^2 chip-on-tip camera compared to the higher quality standard vision reference camera.

Temporal vs. spatial contrast imaging

The results presented highlight the system's capability of capturing physiological blood flow changes *in vivo* with either spatial or temporal contrast imaging. For tracking fast changes like hyperemia, and for measurements involving area-averaging of major parts of the images, spatial contrast is the preferable method. Our results support that temporal contrast is the better processing method for a spatial

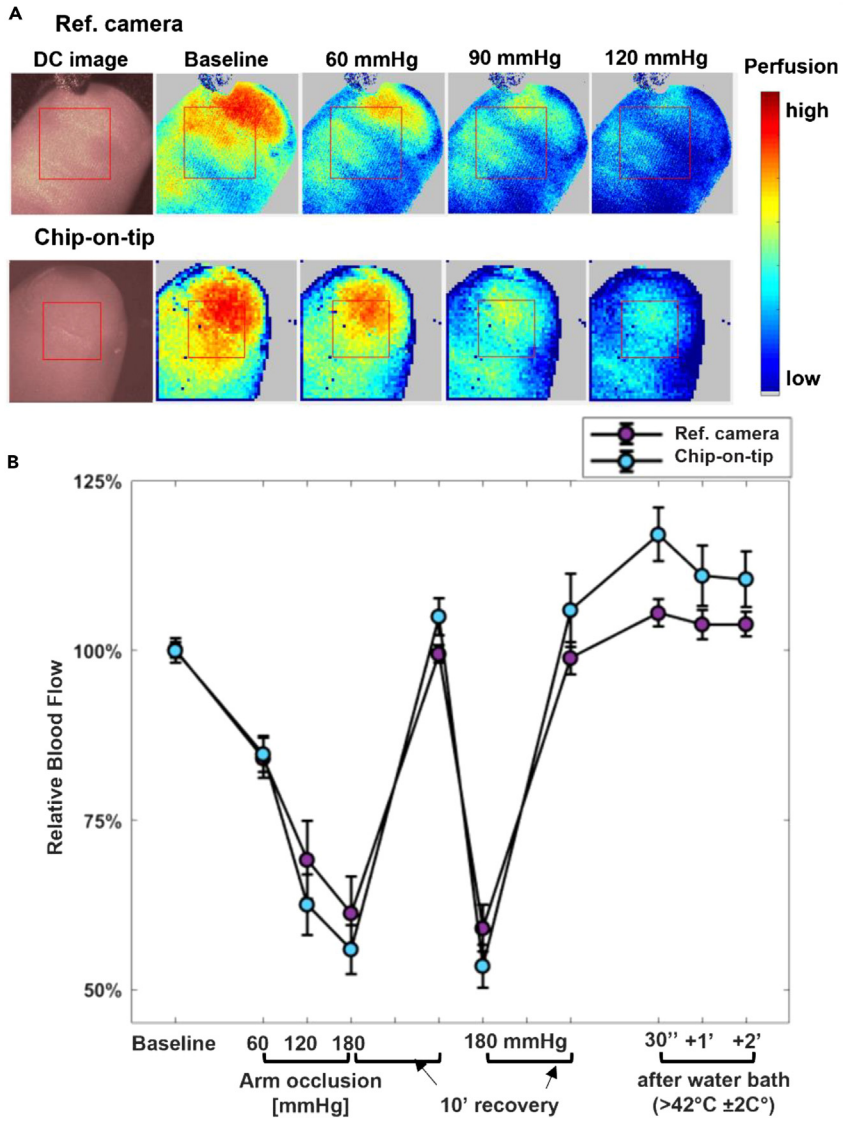

Figure 4. Perfusion of human fingertip using a chip on tip camera

A protocol of physiological blood flow changes captured with speckle contrast imaging in a study of 13 healthy (non-smoking and no known chronic diseases) subjects, imaged with the chip-on-tip camera (AMS) and a secondary reference camera (FLIR).

(A): Representative spatial speckle contrast scans from reference camera (top) and chip-on-tip camera (Bottom, NanEye), under increasing forearm cuff constriction. The underlying monochromatic (DC) imaging (coloring post-processed) and the development during gradual arterial occlusion.

(B): Consolidated blood flow changes (calculated from spatial speckle contrast) in the finger (ROI indicated in A) of 13 subjects for the protocol of restriction, recovery, and temperature stimulation. Mean +/− SEM.

characterization of perfusion and for microvascular mapping. Though the main characteristics were also distinguishable for spatial contrast computation with chip-on-tip, the reduction in number of independent pixels limited the level of detail of such maps. Temporal contrast imaging on the other hand, as demonstrated on imaging fetus *in utero*, provided spatial information at the expense of temporal resolution due to tracking each pixel's intensity fluctuation across 25 consecutive frames (1) and condensing them to one perfusion map.

For assessment of temporal contrast imaging, we conducted two separate experiments. For measuring the flux dependence of linear flow, a flow phantom was developed based on wall-less channels set in an agarose bed. Values captured with chip-on-tip showed an exponential decay in contrast for increasing flow speeds (for 0.1–10 mm/s flow), as did the contrast measured by the reference camera. The result is in agreement with experiments by others[17] and predictions.[34,35] The chip-on-tip recorded contrast value for 1 mm/s flow was higher than expected which could be attributed to the uncertainty related to the generally low contrast levels. Absolute temporal contrast was between 0.052 and 0.065 for the chip-on-tip camera. As for all experiments presented here, the flow phantom measurements were recorded on the

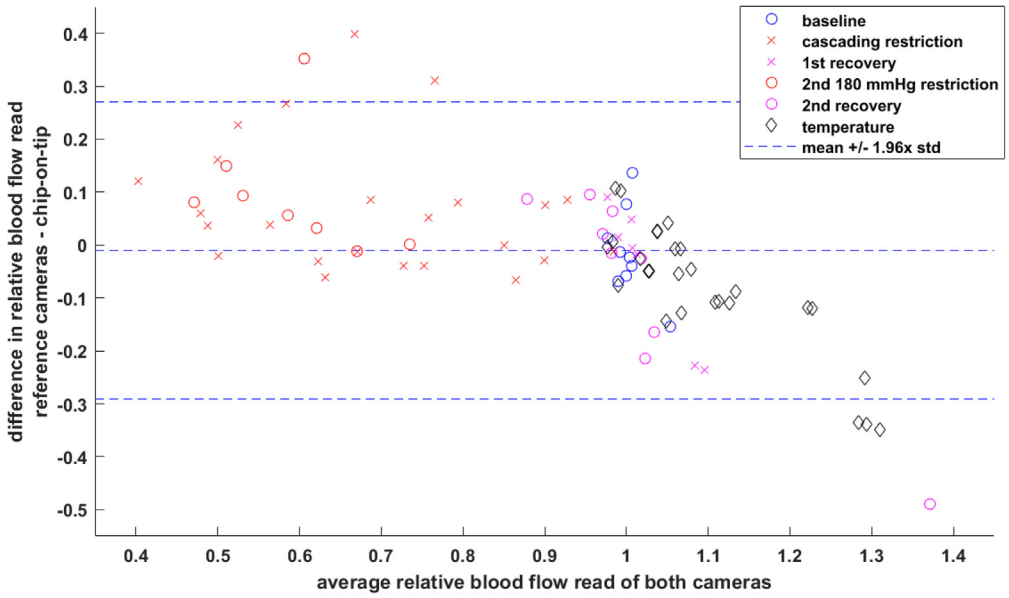

Figure 5. Bland-Altman of the chip-on-tip and reference camera during finger occlusion protocol

Relative blood flow read (spatial contrast converted to perfusion units and baseline-normalized) of the machine vision reference camera and the chip-on-tip micro camera on the fingertip during arterial occlusion, relaxation, and temperature stimulation.

test-rig with a similar optical arrangement. This meant that the imaging optics and especially the resolution at target of 90 μm for chip-on-tip and 21 μm for the reference camera was tuned for producing detailed *in vivo* perfusion maps of the fingertip and the murine placenta *in vivo*. The large size of the target did not adversely affect the calibration tests. However, the flow phantom measurements revealed the limits of the imaging optics. Due to the small diameter of the flow channels (0.75mm) a clear, sharp, separation of the flow area and the static agarose bed was not achieved. The cross-sectional line profiles (Figure 2A) showed a gradual decrease in temporal contrast with minimum values in the center of the channel. Beside the limitation in imaging resolution, the flow phantom images also question the choice of gel bed composition. Previous LSCI studies used a 1% intralipid emulsion for the infused fluid. For the substrate, however, others used PDMS (polydimethylsiloxane) with titanium dioxide seeding,[17,36] which seems to yield better separation of flow and background areas. In order to provide flexibility in the flow phantom characteristics such as channel diameter, depth below the gel surface and distance between the channels, we developed our own phantom design, following the approach of an agarose bed described previously.[10] Figure S1 shows an engineering drawing of the calibration kit to clarify dimensions.

Advancing LSCI into flexible endoscopy

While laser Doppler imaging is firmly embedded in burn wound assessment[8] and laser speckle imaging has been effective in breast reconstructive surgery,[4] the LSCI endoscopy applications are currently confined to pre-clinical research. However, the existing advantages of laser Doppler and LSCI in clinical practice are very encouraging. In burn wound assessment laser Doppler imaging can point to areas which need further treatment, or in words of recent UK NICE report[8]:" to guide treatment decisions for patients in whom there is uncertainty about the depth and healing potential of burn wounds that have been assessed by experienced clinicians". Intraoperative tissue perfusion measurement using LSCI in breast reconstructive surgery has been proven to be promising in several clinical studies.[4,37] Laser Doppler and LSCI are both label free and therefore do not impose logistical constraints that fluorescence-based techniques such as indo-cyanine green (ICG) require (e.g., fluorescence label needs to be administered intravenously). In fact recent multi-centre clinical trial PILLAR III (perfusion assessment in left-sided/low anterior resection)[38] concluded that "the addition of routine indocyanine green fluoroscopy to standard practice adds no evident clinical benefit". The scope of present work is to evaluate chip-on-tip camera in endoscopic context and encourage future applications in flexible endoscopy. The next steps will be to integrate a full endoscopic housing with fiber-coupled laser and chip-on-tip CMOS sensor such as the one shown in the Figure S2.

One of our main goals has been in determining whether the chip-on-tip CMOS camera technologies are adequate for LSCI. NanEye was introduced in 2011 and as mentioned previously, it is surprising neither this nor newer cameras have been evaluated for LSCI. CMOS sensors applied in smartphones and machine vision have found wide use in low light imaging such as night-time closed-circuit TV (CCTV)[39] and advanced fluorescence microscopy.[40] The major issues with off-the shelf cameras are: (1) chip-on-tip cameras are predominantly RGB (red, green, and blue wavelengths) CMOS sensors with NIR (near infrared) blocked (hence standard clinical 785 nm LSCI cannot be done); (2) miniaturization compromises the number of pixels available, and (3) greater noise due to limited space for circuitry and thermal management.

It is encouraging that recent chip-on-tip CMOS sensors are improving rapidly. The chip-on-tip family has been upgraded recently[41] and has more pixels (from 250 × 250 to 320 × 320) with significantly improved noise performance (from 20 e^- temporal dark noise to 6 e−). One important aspect, often overlooked, is the optics performance of the endoscopic lens which defines the working distance, NA, f-number and spatial resolution. The lens in the endoscope can be a separate lens in front of the CMOS sensor with free space in between which is harder to miniaturize and align optically, but designer can optically optimize lens performance for speckle imaging. Parameters such as the speckle size to pixel size ratio to meet the Nyquist sampling criterion of at least 2:1. Alternatively, optics could be integrated on wafer-level lenses which make it intrinsically linked to CMOS electronic sensor and easier to ensure optical alignment and miniature profile. Mass manufacturing of plastic wafer-level lenses combine quality and low cost for large depth-of-field and improved spatial resolution.[42,43] Overall, the capability of the sensors have significantly advanced since early flexible endoscopes incorporated CCD (charge-coupled device) image sensor[44–46] to the smallest ∼0.5 mm sensor recently manufactured.[47]

Limitations of the study

Our study only focused on one chip-on-tip camera as a proof of principle study. Other chip-on-tip cameras could have been compared.

The current study has demonstrated the feasibility of a chip-on-tip camera to image wide-field perfusion map; however, the translation of the findings to provide a specific tool in clinical endoscopic use requires integration into an endoscope. The integration into a flexible endoscope would require alignment of the optic chip-on-tip camera with the light source. Future pre-clinical studies would need to be evaluated alongside the current technology in use "indocyanine green fluoroscopy".

In summary, we demonstrated that coupling a 1mm^2 chip-on-tip camera could achieve accurate perfusion maps by LSCI. This demonstrated the ability in which a chip-on-tip camera can assess comparable LSCI while being ∼1000-times smaller is to a higher quality reference camera (GS3) and was not limited by the lower resolution (249 × 250 pixels vs. 2048 × 1536 pixels) or higher temporal dark noise (50.75 e^- vs. 5.11 e^-) in the chip-on-tip vs. reference camera, respectively. Moreover, the chip-on-tip was accurate in rapidly measuring changes in fingertip perfusion and could confidently measure stepwise decrease in perfusion due to foreman occlusion and slight changes in perfusion attributed to changes in finger temperature. Likewise, the ability of the chip-on-tip camera to provide real time perfusion maps of murine fetus *in utero* demonstrates the potential for translation of this technology for pre-clinical research and clinical settings. Imaging both placenta perfusion and vascular blood flow at a working distance of ∼13 mm shows that it is achievable for integration into a flexible endoscope.

STAR★METHODS

Detailed methods are provided in the online version of this paper and include the following:

- KEY RESOURCES TABLE
- RESOURCE AVAILABILITY
  - Lead contact
  - Materials availability
  - Data and code availability
- METHOD DETAILS
  - Laser speckle contrast imaging system
  - Speckle contrast imaging
  - Image processing
  - Static device validation and calibration
  - Linear flow – dynamic assessment
  - *In vivo* blood flow imaging – human vasculature of the fingertip
  - *In vivo* blood flow imaging – murine pregnancy

SUPPLEMENTAL INFORMATION

Supplemental information can be found online at https://doi.org/10.1016/j.isci.2024.109077.

ACKNOWLEDGMENTS

This project was supported by funding from the European Union's Horizon 2020 research and innovation program under the Marie Skłodowska-Curie grant agreement no 765274, project iPLACENTA. (This publication reflects only the authors' view and that the European Commission and the Research Executive Agency is not responsible for any use that may be made of the information it contains); L.M. PhD is supported by iPlacenta (765274). C.E.M. is coordinator of iPLACENTA and work is also supported by Tenovus Scotland, T18-23.

AUTHOR CONTRIBUTIONS

Conceptualization, C.E.M. and N.K.; methodology, L.M., C.E.M., R.G., and N.K.; software; L.M. and N.K.; formal analysis, L.M. and N.K.; investigation, L.M., N.K., and C.E.M.; resources, C.E.M. and N.K.; data curation, L.M.; writing – original draft, L.M., N.K., and C.E.M.; writing –

review & editing, L.M., C.E.M., R.G., F.K., and N.K.; visualization; L.M., C.E.M., and N.K.; resources, C.E.M. and N.K. ; supervision, C.E.M., N.K., and F.K.; funding acquisition and project administration, C.E.M.

DECLARATION OF INTERESTS

The author R.G. is an employee of Moor Instruments which manufactures and markets Laser imaging technology.

Received: February 8, 2023
Revised: August 28, 2023
Accepted: January 26, 2024
Published: February 1, 2024

REFERENCES

1. Draijer, M., Hondebrink, E., van Leeuwen, T., and Steenbergen, W. (2009). Review of laser speckle contrast techniques for visualizing tissue perfusion. Lasers Med. Sci. *24*, 639–651. https://doi.org/10.1007/s10103-008-0626-3.
2. Tao, S., Zhang, T., Zhou, K., Liu, X., Feng, Y., Zhao, W., and Chen, J. (2022). Intraoperative Monitoring Cerebral Blood Flow During the Treatment of Brain Arteriovenous Malformations in Hybrid Operating Room by Laser Speckle Contrast Imaging. Front. Surg. *9*, 855397.
3. Briers, J.D., and Fercher, A.F. (1982). Retinal blood-flow visualization by means of laser speckle photography. Invest. Ophthalmol. Vis. Sci. *22*, 255–259.
4. To, C., Rees-Lee, J.E., Gush, R.J., Gooding, K.M., Cawrse, N.H., Shore, A.C., and Wilson, A.D.H. (2019). Intraoperative Tissue Perfusion Measurement by Laser Speckle Imaging: A Potential Aid for Reducing Postoperative Complications in Free Flap Breast Reconstruction. Plast. Reconstr. Surg. *143*, 287e–292e. https://doi.org/10.1097/PRS.0000000000005223.
5. Allen, J., and Howell, K. (2014). Microvascular imaging: techniques and opportunities for clinical physiological measurements. Physiol. Meas. *35*, R91–R141. https://doi.org/10.1088/0967-3334/35/7/R91.
6. Ma, K.F., Kleiss, S.F., Schuurmann, R.C.L., Bokkers, R.P.H., Ünlü, Ç., and De Vries, J.-P.P.M. (2019). A systematic review of diagnostic techniques to determine tissue perfusion in patients with peripheral arterial disease. Expert Rev. Med. Devices *16*, 697–710. https://doi.org/10.1080/17434440.2019.1644166.
7. Cosgrove, D., and Lassau, N. (2010). Imaging of perfusion using ultrasound. Eur. J. Nucl. Med. Mol. Imaging *37*, S65–S85. https://doi.org/10.1007/s00259-010-1537-7.
8. NICE (2011). moorLDI2-BI: A laser doppler blood flow imager for burn wound assessment, Guidance, NICE (NICE). Medical technologies guidance. https://www.nice.org.uk/guidance/mtg2.
9. Bray, R.C., Forrester, K.R., Reed, J., Leonard, C., and Tulip, J. (2006). Endoscopic laser speckle imaging of tissue blood flow: Applications in the human knee. J. Orthop. Res. *24*, 1650–1659. https://doi.org/10.1002/jor.20178.
10. dos Santos, G.S., Maneas, E., Nikitichev, D., Barburas, A., David, A.L., Deprest, J., Desjardins, A., Vercauteren, T., and Ourselin, S. (2015). A Registration Approach to Endoscopic Laser Speckle Contrast Imaging for Intrauterine Visualisation of Placental Vessels. In Medical Image Computing and Computer-Assisted Intervention – MICCAI 2015 Lecture Notes in Computer Science, N. Navab, J. Hornegger, W.M. Wells, and A. Frangi, eds. (Springer International Publishing), pp. 455–462. https://doi.org/10.1007/978-3-319-24553-9_56.
11. Heeman, W., Dijkstra, K., Hoff, C., Koopal, S., Pierie, J.-P., Bouma, H., and Boerma, E.C. (2019). Application of laser speckle contrast imaging in laparoscopic surgery. Biomed. Opt Express *10*, 2010–2019. https://doi.org/10.1364/BOE.10.002010.
12. Zheng, C., Lau, L.W., and Cha, J. (2018). Dual-display laparoscopic laser speckle contrast imaging for real-time surgical assistance. Biomed. Opt Express *9*, 5962–5981. https://doi.org/10.1364/BOE.9.005962.
13. Chen, M., Wen, D., Huang, S., Gui, S., Zhang, Z., Lu, J., and Li, P. (2018). Laser speckle contrast imaging of blood flow in the deep brain using microendoscopy. Opt. Lett. *43*, 5627–5630. https://doi.org/10.1364/OL.43.005627.
14. Song, L., and Elson, D.S. (2012). Dual-wavelength endoscopic laser speckle contrast imaging system for indicating tissue blood flow and oxygenation. In Proc. SPIE 8222, Dynamics and Fluctuations in Biomedical Photonics IX (SPIE), pp. 34–41. https://doi.org/10.1117/12.908241.
15. Flusberg, B.A., Cocker, E.D., Piyawattanametha, W., Jung, J.C., Cheung, E.L.M., and Schnitzer, M.J. (2005). Fiber-optic fluorescence imaging. Nat. Methods *2*, 941–950. https://doi.org/10.1038/nmeth820.
16. Wang, J., and Nadkarni, S.K. (2014). The influence of optical fiber bundle parameters on the transmission of laser speckle patterns. Opt Express *22*, 8908–8918. https://doi.org/10.1364/OE.22.008908.
17. Regan, C., White, S.M., Yang, B.Y., Takesh, T., Ho, J., Wink, C., Wilder-Smith, P., and Choi, B. (2016). Design and evaluation of a miniature laser speckle imaging device to assess gingival health. J. Biomed. Opt. *21*, 104002. https://doi.org/10.1117/1.JBO.21.10.104002.
18. Lotay, A.S., and Girkin, J.M. (2019). Towards a portable laser speckle based device to evaluate the level of atrophy in tissue. In Design and Quality for Biomedical Technologies XII, R. Liang and J. Hwang, eds. (SPIE)), pp. 29–40. https://doi.org/10.1117/12.2507845.
19. Huang, C., Gu, Y., Chen, J., Bahrani, A.A., Abu Jawdeh, E.G., Bada, H.S., Saatman, K., Yu, G., and Chen, L. (2019). A Wearable Fiberless Optical Sensor for Continuous Monitoring of Cerebral Blood Flow in Mice. IEEE J. Sel. Top. Quantum Electron. *25*, 6900108. https://doi.org/10.1109/JSTQE.2018.2854597.
20. Murdoch, C.E., Shuler, M., Haeussler, D.J.F., Kikuchi, R., Bearelly, P., Han, J., Watanabe, Y., Fuster, J.J., Walsh, K., Ho, Y.-S., et al. (2014). Glutaredoxin-1 Up-regulation Induces Soluble Vascular Endothelial Growth Factor Receptor 1, Attenuating Post-ischemia Limb Revascularization. J. Biol. Chem. *289*, 8633–8644. https://doi.org/10.1074/jbc.M113.517219.
21. McNeilly, A.D., Gallagher, J., McCrimmon, R.J., Gomez, M.F., and Khan, F. (2015). NFAT inhibition improves microvascular function in a mouse model of chronic diabetes. Atherosclerosis *241*, e145. https://doi.org/10.1016/j.atherosclerosis.2015.04.502.
22. Armitage, G.A., Todd, K.G., Shuaib, A., and Winship, I.R. (2010). Laser Speckle Contrast Imaging of Collateral Blood Flow during Acute Ischemic Stroke. J. Cereb. Blood Flow Metab. *30*, 1432–1436. https://doi.org/10.1038/jcbfm.2010.73.
23. Sigal, I., Koletar, M.M., Ringuette, D., Gad, R., Jeffrey, M., Carlen, P.L., Stefanovic, B., and Levi, O. (2016). Imaging brain activity during seizures in freely behaving rats using a miniature multi-modal imaging system. Biomed. Opt Express *7*, 3596–3609. https://doi.org/10.1364/BOE.7.003596.
24. Miao, P., Lu, H., Liu, Q., Li, Y., and Tong, S. (2011). Laser speckle contrast imaging of cerebral blood flow in freely moving animals. J. Biomed. Opt. *16*, 090502. https://doi.org/10.1117/1.3625231.
25. Miao, P., Zhang, L., Li, M., Zhang, Y., Feng, S., Wang, Q., and Thakor, N.V. (2017). Chronic wide-field imaging of brain hemodynamics in behaving animals. Biomed. Opt Express *8*, 436–445. https://doi.org/10.1364/BOE.8.000436.
26. Senarathna, J., Yu, H., Deng, C., Zou, A.L., Issa, J.B., Hadjiabadi, D.H., Gil, S., Wang, Q., Tyler, B.M., Thakor, N.V., and Pathak, A.P. (2019). A miniature multi-contrast microscope for functional imaging in freely behaving animals. Nat. Commun. *10*, 99. https://doi.org/10.1038/s41467-018-07926-z.
27. Senarathna, J., Murari, K., Etienne-Cummings, R., and Thakor, N.V. (2012). A Miniaturized Platform for Laser Speckle Contrast Imaging. IEEE Trans. Biomed. Circuits Syst. *6*, 437–445. https://doi.org/10.1109/TBCAS.2012.2218106.
28. Ringuette, D., Jeffrey, M.A., Dufour, S., Carlen, P.L., and Levi, O. (2017). Continuous multi-modality brain imaging reveals modified neurovascular seizure response after intervention. Biomed. Opt Express *8*,

873–889. https://doi.org/10.1364/BOE.8.000873.
29. Song, L., and Elson, D.S. (2013). Effect of signal intensity and camera quantization on laser speckle contrast analysis. Biomed. Opt Express *4*, 89–104. https://doi.org/10.1364/BOE.4.000089.
30. Yang, O., and Choi, B. (2012). Laser speckle imaging using a consumer-grade color camera. Opt. Lett. *37*, 3957–3959. https://doi.org/10.1364/OL.37.003957.
31. Postnov, D.D., Cheng, X., Erdener, S.E., and Boas, D.A. (2019). Choosing a laser for laser speckle contrast imaging. Sci. Rep. *9*, 2542. https://doi.org/10.1038/s41598-019-39137-x.
32. Wu, C., and Bayer, C.L. (2018). Imaging placental function: current technology, clinical needs, and emerging modalities. Phys. Med. Biol. *63*, 14TR01. https://doi.org/10.1088/1361-6560/aaccd9.
33. Yuan, S., Devor, A., Boas, D.A., and Dunn, A.K. (2005). Determination of optimal exposure time for imaging of blood flow changes with laser speckle contrast imaging. Appl. Opt. *44*, 1823–1830. https://doi.org/10.1364/AO.44.001823.
34. Ramirez-San-Juan, J.C., Mendez-Aguilar, E., Salazar-Hermenegildo, N., Fuentes-Garcia, A., Ramos-Garcia, R., and Choi, B. (2013). Effects of speckle/pixel size ratio on temporal and spatial speckle-contrast analysis of dynamic scattering systems: Implications for measurements of blood-flow dynamics. Biomed. Opt Express *4*, 1883–1889. https://doi.org/10.1364/BOE.4.001883.
35. Boas, D.A., and Dunn, A.K. (2010). Laser speckle contrast imaging in biomedical optics. J. Biomed. Opt. *15*, 011109. https://doi.org/10.1117/1.3285504.
36. Richards, L.M., Kazmi, S.M.S., Davis, J.L., Olin, K.E., and Dunn, A.K. (2013). Low-cost laser speckle contrast imaging of blood flow using a webcam. Biomed. Opt Express *4*, 2269–2283. https://doi.org/10.1364/BOE.4.002269.
37. Zötterman, J., Opsomer, D., Farnebo, S., Blondeel, P., Monstrey, S., and Tesselaar, E. (2020). Intraoperative Laser Speckle Contrast Imaging in DIEP Breast Reconstruction: A Prospective Case Series Study. Plast. Reconstr. Surg. Glob. Open *8*, e2529. https://doi.org/10.1097/GOX.0000000000002529.
38. Jafari, M.D., Pigazzi, A., McLemore, E.C., Mutch, M.G., Haas, E., Rasheid, S.H., Wait, A.D., Paquette, I.M., Bardakcioglu, O., Safar, B., et al. (2021). Perfusion Assessment in Left-Sided/Low Anterior Resection (PILLAR III): A Randomized, Controlled, Parallel, Multicenter Study Assessing Perfusion Outcomes With PINPOINT Near-Infrared Fluorescence Imaging in Low Anterior Resection. Dis. Colon Rectum *64*, 995–1002. https://doi.org/10.1097/DCR.0000000000002007.
39. Brown, E. (2019). Optimizing Image Sensors for Security Cameras. Photonics Imaging Technol.
40. Diekmann, R., Till, K., Müller, M., Simonis, M., Schüttpelz, M., and Huser, T. (2017). Characterization of an industry-grade CMOS camera well suited for single molecule localization microscopy – high performance super-resolution at low cost. Sci. Rep. *7*, 14425. https://doi.org/10.1038/s41598-017-14762-6.
41. AMS NanEyeC Smallest Integrated Camera Module. Ams. https://ams.com/en/naneyec.
42. Voelkel, R. (2012). Wafer-scale micro-optics fabrication. Adv. Opt. Technol. *1*, 135–150. https://doi.org/10.1515/aot-2012-0013.
43. Waeny, M.. Mini Camera Modules Pave Way for Less-Invasive Visualization. https://www.photonics.com/Articles/Mini_Camera_Modules_Pave_Way_for_Less-Invasive/a56663.
44. Sivak, M.V., Jr., and Fleischer, D.E. (1984). Colonoscopy with a VideoEndoscope: preliminary experience. Gastrointest. Endosc. *30*, 1–5. https://doi.org/10.1016/s0016-5107(84)72282-6.
45. Classen, M., and Phillip, J. (1984). Electronic endoscopy of the gastrointestinal tract. Initial experience with a new type of endoscope that has no fiberoptic bundle for imaging. Endoscopy *16*, 16–19. https://doi.org/10.1055/s-2007-1018518.
46. De Groen, P.C. (2017). History of the Endoscope [Scanning Our Past]. Proc. IEEE *105*, 1987–1995. https://doi.org/10.1109/JPROC.2017.2742858.
47. OVMed OVMed Medical Image Sensor Is World's Smallest Commercial Sensor | Imaging and Machine Vision Europe. https://www.imveurope.com/press-releases/ovmed-medical-image-sensor-worlds-smallest-commercial-sensor.
48. Goodman, J.W. (1975). Statistical Properties of Laser Speckle Patterns. In Laser Speckle and Related Phenomena Topics in Applied Physics, J.C. Dainty, ed. (Springer), pp. 9–75. https://doi.org/10.1007/978-3-662-43205-1_2.
49. Goodman, J.W. (2020). Speckle Phenomena in Optics: Theory and Applications, Second Edition (SPIE Press).
50. Bezemer, R., Klijn, E., Khalilzada, M., Lima, A., Heger, M., van Bommel, J., and Ince, C. (2010). Validation of near-infrared laser speckle imaging for assessing microvascular (re)perfusion. Microvasc. Res. *79*, 139–143. https://doi.org/10.1016/j.mvr.2010.01.004.

STAR★METHODS

KEY RESOURCES TABLE

REAGENT or RESOURCE	SOURCE	IDENTIFIER
Experimental models: Organisms/strains		
C57/BL6 Charles River		
Software and algorithms		
Matlab Educational (R2023a), Mathworks, UK	R version 3.5.3, www.r-project.org	V5

RESOURCE AVAILABILITY

Lead contact

Further information and requests for resources and information should be directed to and will be fulfilled by Colin Murdoch, (c.z.murdoch@dundee@ac.uk).

Materials availability

"This study did not generate new unique materials."

Data and code availability

"The datasets and Matlab code generated in this study is available on request by contacting Colin Murdoch, (c.z.murdoch@dundee@ac.uk)

METHOD DETAILS

Laser speckle contrast imaging system

The imaging system was designed and built for the assessment of miniaturized LSCI hardware based on the chip-on- tip camera NanEye (NE2D_B&W_FOV90F2.7_2m, AMS, Austria) and fiber- coupled laser illumination (Figure 1A). The setup allowed positioning of the small 1 × 1 mm footprint NanEye camera (Figure 1B), adjustability of the camera-object distance and optimized laser light illumination. A secondary standard machine vision reference camera (GS3-U3-32S4M-C, Teledyne FLIR, USA) was incorporate into the set-up for reference imaging of the laser speckle pattern. The camera specifications of the two cameras are compared in Table 1.

A fiber-coupled, Volume-Holographic-Grating- (VHG) stabilized, 785 nm laser (LP785-SAV50, Thorlabs Ltd, UK) was chosen for illumination due to suitable coherence stability which had previously been validated for LSCI application.[31] After exiting the single mode fiber connected to the laser diode, the near-infrared light passed through a linear polarizer (LPNIRE100-B, Thorlabs, UK) and then directed by a mirror (BB1-E02P, Thorlabs, UK) onto the target. The backscattered portion of light passed through a second, orthogonally aligned polarizer (LPNIRE2X2, Thorlabs, UK) before entering the chip-on-tip camera. Similarly, the capture of the reference camera was also cross-polarized (LPNIRE100-B, Thorlabs, UK) and used a mirror (BB1-E02P, Thorlabs, UK) to adjust alignment. Figure 1 and Table 1 list the key components and their properties.

The laser diode driver was a CLD1010LP laser controller (Thorlabs Ltd, UK). Peak optical power output was limited to 4.9 mW (measured after the first polarizer) by a variable optical attenuator (VOA 1064-APC, Thorlabs Ltd, UK). To ensure laser safety and to eliminate ambient light from interfering with the laser speckle pattern, the LSCI setup was enclosed in a blacked-out box with a curtain for manual access. A mold ensured accurate positioning and tissue stability for the fingertip measurements.

The chip-on-tip camera was positioned at optimal focal distance of 13 mm from the target and imaged via an integrated lens (f/# = 2.7) with a 90° FOV. The reference camera was placed at 350 mm distance and combined with a 50 mm fixed focal length lens (MVL50M23, Thorlabs Ltd, UK). Both cameras captured at 40 fps with 25 ms exposure time. The chip-on-tip camera had the gain setting set to 6.5dB and offset setting set to 2 for all experiments. The gain and offset are manufacturer specific camera settings directly regulating the CMOS sensor's analog-to-digital converters gain and offset. For each step of the fingertip vasculature protocol, a series of 100 raw images were recorded. Equally we recorded 100 frames for each flow speed for the flow phantom measurements. Proprietary control software was used for the reference camera (PointGrey Research, FlyCap 2.13.3.61); a custom MATLAB (R2018a, Mathworks, UK) interface was developed for chip-on-tip. This allowed the recording of sequences of raw image data for each camera, at 5s intervals.

Speckle contrast imaging

Imaging of vascular activity by LSCI techniques relies on spatial and temporal statistical characterization of laser speckles. When coherent light backscatters off a diffusing surface, it forms a random interference pattern called laser speckles. Moving objects, such as red blood cells in tissue, cause fluctuations and blurring of the pattern within a set exposure duration. Goodman's work linked the variance of a time-averaged

dynamic speckle pattern and the temporal fluctuation statistics.[48,49] Fercher and Briers then applied the principle for blood flow imaging in single exposure photography.[3] Nowadays, the speckle pattern is mostly captured by imaging sensors, i.e. an array of pixels measuring repeatedly the intensity of backscattered light. Speckle contrast, K, was defined as the quotient of the standard deviation (σ) of the recorded intensities and the average intensity (I):

$$K = \sigma / \langle I \rangle. \quad \text{(Equation 2)}$$

For spatial processing, a single image was analyzed by calculating speckle contrast for a small cluster of pixels (5 × 5). For temporal contrast imaging, the intensity fluctuation of each pixel was analyzed for a sequence of 100 frames.

Image processing

Images captured by the chip-on-tip camera and the standard vision reference camera and were post-processed and calculated perfusion maps were developed using a custom MATLAB script. Spatial speckle contrast was determined framewise for a 5 × 5 pixel stepping window, hence reducing the spatial resolution of the resulting perfusion map. Temporal speckle contrast on the other hand was determined by a 25-frame sliding kernel, thus quantifying the temporal intensity fluctuation of each pixel. Both speckle contrast calculation methods were used for the image data of both cameras. The perfusion maps calculated from 100 intensity images were time-averaged.

Static device validation and calibration

A commercial motility reference (based on Brownian motion and manufactured by Moor Instruments Ltd, UK) was used to calibrate the resolvable speckle contrast range for the chip-on-tip LSCI setup. The calibration consisted of two vials, one for static contrast reference and the second vial as a motility standard as it was filled with an aqueous suspension of monodisperse polystyrene microspheres. A custom-designed, 3D-printed holder positioned the two vials at 13mm imaging distance for the Chip-on-tip camera. The calibration kit defined the conversion of speckle contrast to arbitrary perfusion units (PU), with the reflector vial provided a zero reference and the motility vial set at 500 PU.

Optimum speckle contrast was achieved by measurement assessments over a range of settings, varying target distance (8, 10 mm, 12 mm, 20 mm), laser illumination power (1 mW, 3 mW, 5 mW), exposure time (5 ms, 15 ms, 25 ms) and chip-on-tip gain (1dB, 2.4dB, 6.5dB). The position of the reference camera was kept constant at 350 mm distance, the exposure time and the illumination power were varied equally to the chip-on-tip. For the chip-on-tip, a 50 × 50 pixel area was chosen in the center region of each vial to determine spatial contrast. The ROIs were area-matched on the reference camera images (equal to 150 × 150 pixel windows). Spatial contrast was computed for both cameras using a 5 × 5 pixel kernel and averaging 100 contrast maps.

Linear flow – dynamic assessment

Measurements were conducted on a flow phantom to test the LSCI system's capability of detecting linear flow, and to assess temporal contrast capture. The phantom was based on a design previously described[10] for wall-less channels in a gel bed. A mold was designed and 3D-printed featuring inlet ports in the front wall and outlet ports in the back wall. For the channel creation Nylon wires were tensioned between the ports and a 5.5% (w/v) agarose bed with 0.5% (v/v) intralipid seeding was poured into the mold. After curing the bed, the wires were removed through the inlet ports, creating straight, wall-less channels. We used 0.75 mm channels positioned 1mm below the bed surface. A 1% (v/v) intralipid emulsion was infused through 1.1mm hypodermic needles with needle tip embedded in the gel. Each channel was individually supplied and controlled by a separate syringe pump (70-2001 Harvard Apparatus, US). Figure 2 displays the flow phantom setup. Speckle contrast was imaged for 0.1, 0.5, 1, 5 and 10 mm/s flow speeds. For each condition 50 frames were capture at 25ms exposure by the chip-on-tip and the reference camera. Laser illumination was set to 3mW output power and cross-polarized. Chip-on-tip was positioned at 13 mm distance to the agarose bed (the reference camera was positioned at ≈350mm distance as described in section 2.1). Temporal contrast was computed from 25 frames for an ROI of 100 x 30 pixels (including the channel) for chip-on-tip camera, and 200 x 50 pixels for the reference camera. The perfusion data of 50 intensity images was averaged.

In vivo blood flow imaging – human vasculature of the fingertip

An *in vivo* study to image vasculature in the fingertip of human volunteers (or subjects) was approved by the ethics research committee of the School of Medicine at the University of Dundee, Scotland, and informed consent was obtained (SMED REC Number 21/ 66). 13 healthy (non-smoking and no known chronic diseases) subjects (7 males, 6 females) were recruited within an age range of 20-60.

The objective of this study was the assessment of the chip-on-tip LSCI hardware measuring physiological blood flow changes. A protocol previously described by others[17,50] was adapted to measure changes in fingertip perfusion induced by pressure cuff on the upper arm, see Table 2. All subjects were in a seated position and allowed to acclimatize for at least 10 minutes before readings took place. The subject's ring or middle finger was carefully placed under the imaging setup with the nailfold facing upwards, i.e. towards the cameras. The subject's arm and hand were supported to ensure maximum comfort so the subject would not move the finger during imaging. For each protocol step, both cameras imaged the fingertip for 2.5 s. Measurements were always taken of the same finger for each person, either the middle or the ring finger. A finger was chosen to minimise positioning and movement of the imaging system between subjects. Blood flow is unlikely to be dramatically different between two fingers and all measurements in this study are relative blood flow response measurements. The ambient temperature of the experimental room was maintained at 21 ± 2°C.

Four sets of baseline scans were recorded before a pressure cuff on the subject's upper arm was inflated consecutively to 60 mmHg, 120 mmHg and 180 mmHg occlusion pressure. For each level the pressure was held for 30 s before acquiring the image data. After the maximum occlusion, pressure was released. Five sets of measurements were taken within the first minute of the occlusion release by chip-on-tip camera to capture hyperemia. Following 10 min of recovery, the perfusion level was measured. The upper arm pressure cuff was then inflated directly to 180 mmHg and held for 90 s with subsequent measurement. Pressure was then released, and recovery perfusion measured after 10 min. (Also, hyperemia was captured by the reference camera). In a last stage the subject's entire hand was immersed into a water bath with the temperature at 42°C ± 2°C. After 5min the hand was taken out of the water, quickly dried to remove any reflecting water, and then scanned. Three measurements were taken after heating with 1 min between the scans. Recordings of the reference camera were conducted following the chip-on-tip captures for all conditions within a 5 sec time window.

In vivo blood flow imaging – murine pregnancy

To test imaging *in vivo* vasculature imaging, we imaged placental, fetal and uterine blood flow in pregnant C57Bl6 mice. Animal studies carried out in this study were approved and regulated by UK Government Home Office in accordance with the "Guidance on the operation of Animals' (Scientific Procedures) Act, 1986, in agreement with University of Dundee institutional guidelines and regulations for ethical animal use and care. The uterus of sedated (isoflurane) pregnant mice was exposed on day 17.5 of gestation, containing multiple fetus and placenta. Each amniotic sac contains a fetus and placenta surrounded by amnionic fluid. The maternal vasculature of the maternal horn is connected to the fetus via the placenta. Two amniotic sacs were individually placed under the micro camera of the LSCI set-up. The camera-to-object distance was 10 mm. A surgical vascular clamp was used to transiently ligate the maternal arteries in the uterine horn supplying the individual exposed placenta. We captured laser speckle contrast prior to the constriction and 30 seconds into ligation. Sets of 100 images at 25 ms exposure were acquired for each condition. The LSCI imaging was performed under 785 nm illumination at 4.9 mW. At the end of the procedure the mice were euthanized.